International Journal of Material Forming (2021) 14:703–714
https://doi.org/10.1007/s12289-020-01565-w

ORIGINAL RESEARCH

Numerical simulation of self heating during stretch blow moulding of PET: viscohyperelastic modelling versus experimental results

Yun-Mei Luo[1] · Luc Chevalier[1] · Eric Monteiro[2] · Françoise Utheza[1]

Received: 17 January 2020 / Accepted: 28 April 2020 / Published online: 27 May 2020

Abstract
During the stretch blow moulding (SBM) process of polyethylene terephthalate (PET) bottle, high viscous dissipation generates self heating phenomena. Since the influence of temperature on polymer's behavior is important, it is necessary to evaluate the self heating values in order to manage accurately the simulation of the process. An anisotropic visco-hyperelastic model has been developed to manage numerical simulations of free blowing. The model takes into account the anisotropy and the effect of the temperature. It has been computed in a user-interface VUMAT implemented in the software ABAQUS/Explicit. The identification of the model is based on experimental data of biaxial tension tests. We identified the characteristics taking into account the self-heating effect by a semi analytical process followed by an adjustment using finite element. For sake of validation, PET preforms have been blown from different initial temperature and followed using a thermal camera. The increase of temperature is measured by comparing initial temperature and final temperature. Comparison between the experimental and numerical simulations is discussed and influence of initial temperature or blowing pressure is highlighted in a large numerical investigation.

Keywords Self-heating · Experimental results · Numerical simulation · Free blowing process

Introduction

The ISBM process is widely used in the bottling industry to produce PET bottles. This process is managed at a temperature slightly above the glass transition temperature Tg before stretching and inflating inside a bottle mould. Multiple research groups, industrial or academic, have examine the deformation of PET during the ISBM process. Their goal was to comprehend and to model the procedure using numerical simulation. Therefore, numerous approaches have been developed during the 20 last years [1–7]. The microstructural morphology of PET strongly affects the thermal behavior of the PET during the process. This in turn affects the distribution of the temperature of final bottle, thickness, crystallinity and orientation. These distributions are responsible for the final products' mechanical properties [8, 9]. An increase of temperature allows chain mobility and relaxation reduces the extension of macromolecular chains [10]. The effects of temperature and heating conditions that have a fundamental importance during ISBM process are the topic of this study.

Regarding the experimental approach, some experimental methods [11–13] were among the first study on the PET sheet where the geometry is less complex than a preform. Through their researches, the thermal parameters of the infrared oven and the interaction between the emitter and the PET sheet can be characterized. Later, for the preform case, Huang et al. [14] investigated the use of thermocouples inserted into the preform thickness. Nevertheless, this method remains highly delicate. Recently, Salomeia et al. [15] and Menary [16] did the temperature measurements of the air blown inside the bottle. Their experimental work provided numerous data for the thermal boundary conditions for the ISBM simulations. Temperature was measured using a thermocouple junction mounted in the metallic stretch rod with a silicon sealant. The evolution of the mean temperature of the blown air blown in the hot preform can then be determined.

Besides, the numerical approach has seen a rapid growth in the last decade. Different models were implemented into commercial finite element code [17, 18]. Others developed

✉ Yun-Mei Luo
yunmei.luo@univ-paris-est.fr

[1] Laboratoire Modélisation et Simulation Multi Echelle, MSME UMR 8208 CNRS, Université Paris-Est, Marne-la-Vallée, France

[2] PIMM, Arts et Metiers Institute of Technology, CNRS, Cnam, HESAM University, 151 boulevard de l'Hopital, 75013 Paris, France

their own software [13, 19–21] to predict the preform temperature distribution. In previous papers [22, 23], we also, have presented a contribution on the thermal aspects of the ISBM process: the identification procedure of the thermal properties of PET sheets from IR heating tests including the natural air convection effect. More recently, an accurate thermal boundary condition has been provided to perform a 3D thermal finite element simulation of the infrared heating [24]. In the stretch blowing stage, numerous reliable and robust simulations of the ISBM process has been managed in order to produce any desired bottle shape [2, 4, 25–29]. This simulation is generally conducted using some form of finite element solver. The classical viscoelastic models such as the Upper Convected Maxwell model [30, 31] do not adequately demonstrate the strain hardening effect during the ISMN process. Schmidt et al. [25] used a viscoelastic model taking into account the strain hardening effect in ISBM simulation and developed a non-isothermal finite element simulation to embed heat transfer during the deformation process. The prediction of the thickness distribution was not significantly improved and these simulations did not show areal improvement the force evolution exerted by the stretch rod. Later, Menary et al. [26, 29] applied a nonlinear viscoelastic model (Buckley's model) [32] in the ISBM simulation using the finite element package ABAQUS/standard and showed fine agreement with thickness distribution and bubble evolution. Here, we present a different type of visco-hyperelastic modelling coupled to temperature in order to simulate the self-heating phenomena.

In the first part of this work, we recall some results on an experimental study: we have partially presented, in a previous publication [7], results on free blowing of preforms managed at various initial temperatures and blowing pressures. Infrared camera was used to capture the temperature field and comparing the initial and final values in the same area of the PET preform, we evaluate the increase of temperature due to deformation of the preform. We focus on bubble that have the same inside volume to characterize the self-heating phenomenon.

In the second section, a numerical study of the free blow case is performed. We identified the properties of the visco-hyperelastic model previously presented in its orthotropic version in [33]. It has been extended here, to be coupled with the thermal equation and is used to characterize the PET behavior. It has been done from experimental data issued from biaxial tension tests and taking into account the self-heating effect. We have computed and implemented our model via a user-interface VUMAT, into the software ABAQUS and we performed free blowing simulations. The effect of the temperature and the induced anisotropy are taken into account in these simulations. Both numerical and experimental results of the self heating phenomena are compared and discussed in the last section.

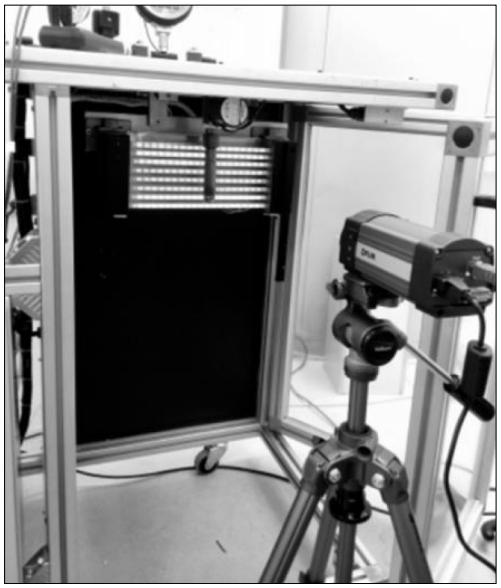

Fig. 1 Experimental set-up for free blowing: preform is heated by 8 infrared lamps and a thermal camera is used to measure the evolution of temperature

Experimental study of free blowing case

Injected preforms designed for carbonated soft drinks are provided by SIDEL. They are used to study the self heating phenomena. We prepare these preforms by heating it with 8 infrared lamps in order to provide different initial thermal conditions. A free blowing apparatus developed at laboratory MSME (Fig. 1) allows to produce different blowing pressure. The temperature distribution on the external surface of the preform was measured using a FLIR B250 infrared camera. The camera's wavelength range is 7.5–13 μm and is used to follow the evolution of the preform during the entire blowing process. The PET material is opaque under the wavelength in the range of 8–12 μm. The assumption is made of a constant emissivity value for this temperature level.

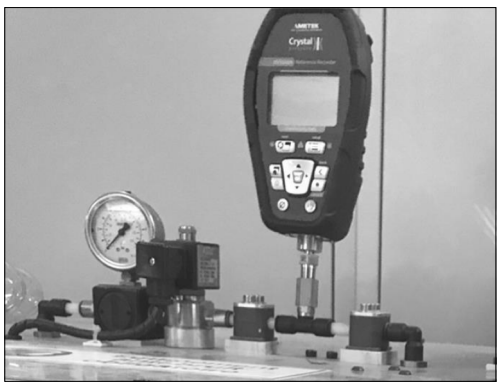

Fig. 2 Manometer for measuring the pressure

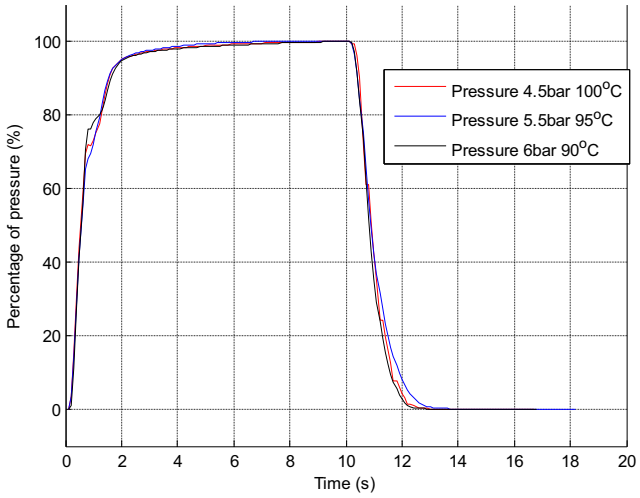

Fig. 3 Evolution of pressure during the blowing stage

For the pressure measurement, we use the manometer shown on Fig. 2. The sampling rate of this manometer is 10 values of pressure per second.

Figure 3 shows under different heating temperature, the pressure rise rate is same to obtain the setting pressure. The history of pressure can be implemented as the boundary condition in the numerical simulation.

Table 1 shows the different initial temperature and the different pressure condition used to obtain similar final elongation. Temperature is measured from thermal camera that gives the outside surface temperature. This temperature can be very different from the inside surface one at the beginning of the process but the bubble thickness becomes very small and we can assume the final temperature is uniform in the thickness direction.

The volume of a bottle is measured from the weight of the water needed to fill the bottle. Higher the initial temperature is lower pressure is needed for the same volume of bottle. The cross means the exploded case.

Furthermore, the longitudinal and circumferential elongations λ_z and λ_θ are measured by comparing the distance between regular spots on the preform and the same ones on the blown bottle. As presented in [7], biaxial elongations are measured from an initial grid drawn on the preform before blowing and measured after blowing. In Table 1, mean values of these elongations are listed in different region of the bottle for the selected tests. The circumferential elongation in the center part is around 4 for 85 °C, 100 °C and 105 °C, and it equals 3.5 for the 90 °C and 95 °C. This value is about 1.5 times larger than the longitudinal elongation (2.5 for all cases). Longitudinal and circumferential elongation difference induces anisotropy in the morphology of the PET material during the process that must be taken into account if one needs to model the blowing process. It also induces anisotropy in the mechanical properties, especially longitudinal and circumferential elastic modulus are different.

Temperature measurements during free blowing of PET preform is illustrated on Fig. 4. We determine the increase of temperature by comparison between the initial temperature in three zones located near the neck, in the middle of the preform height, near the bottom; with the final temperature in these three zones located near the neck, in the middle of the bottle height and near the bottom.

Table 2 gives the increase of temperature in these three zone for different initial temperature. One can see that the self heating phenomena can lead to 18 °C of increase of the temperature and does not vary significantly from different zone and different initial temperature. In particular, zone 5–6 has a bigger elongation in the hoop direction and also an initial temperature lower than in other region of the preform. Consequently, the increase is higher in this zone.

The mean difference does not exceed 20% and this means that initial temperature has not an important effect on the self heating phenomena.

Table 1 Measured elongations of blown preform in longitudinal and circumferential directions

Case		85 °C, 7 bar	90 °C, 6 bar	95 °C, 5.5 bar	100 °C, 4.5 bar	105 °C, 2.5 bar
Elongations						
Experimental	λ_θ top	4.5	4.5	4.8	4.2	4.5
	λ_θ center	4	3.5	3.5	4	4
	λ_θ bottom	4	3.8	3.5	4.3	4
	λ_z top	3.5	4	3.5	4	3.5
	λ_z center	2.5	2.5	2.5	2.5	2.5
	λ_z bottom	3.2	3.5	3.5	3.5	3.7
	Final volume (ml)	920	895	880	900	950

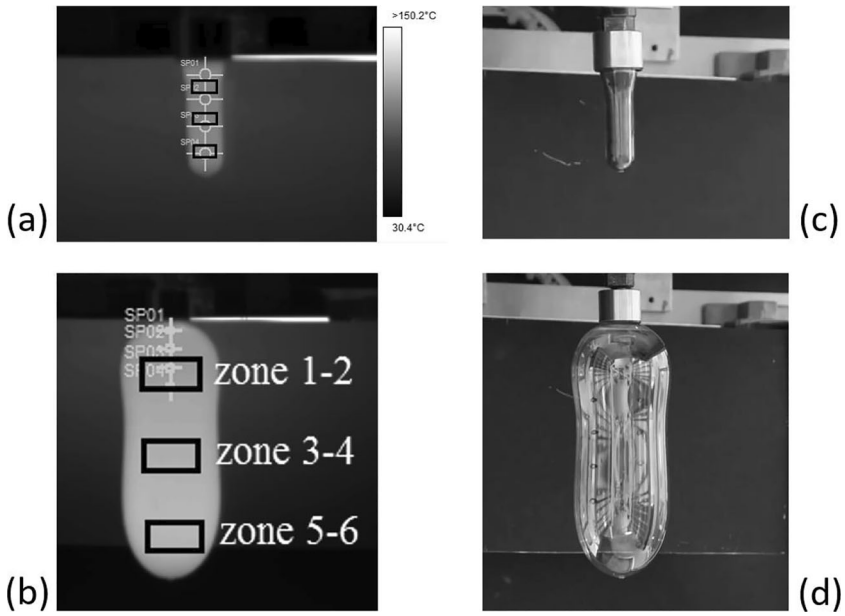

Fig. 4 Pictures of temperature field and strain measurements during free blowing of PET preform.**a** Snapshot of the temperature field and location of area where initial temperature is measured, **b** large rectangles on the final bottle give the corresponding final temperature, **c** preform captured from classical camera, black spots are regularly drawn on the preform, **d** blown bottle: dark spots enable the evaluation of the stretch ratio for each direction longitudinal and circumferential

Temperature-dependent viscohyperelastic model

The non linear incompressible visco-hyperelastic (VHE) model has been presented and identified in author's previous publications [6, 22]. Our isotropic version of the model failed to predict the correct aspect ratio between length and radius of the blown bottle so an anisotropic version has been developed. The anisotropy is introduced in both the viscous and elastic parts of the model in order to represent the strain hardening effect that appears during elongations at this temperature slightly over T_g [24]. The anisotropic version of the VHE model has a Maxwell like form in finite strain.

For the elastic part, the strain hardening effect needs to be represented by an exponential function of elongation so we choose a Hart-Smith like model for this part. We use invariants of the elastic left Cauchy Green tensor $\underline{\underline{B_e}}$ associated to the isotropic and anisotropic material behavior have to be defined to build the model. I_1, I_2 and I_3 are the classical invariants, and I_4, I_5 and I_6 are associated to the anisotropic behavior.

$$I_1 = tr\left(\underline{\underline{B_e}}\right),\ I_2 = \frac{1}{2}\left[tr\left(\underline{\underline{B_e}}\right)^2 - tr\left(\underline{\underline{B_e}}^2\right)\right],\ I_3 = \det\left(\underline{\underline{B_e}}\right),$$
$$I_4 = \underline{n_1}\cdot\underline{\underline{B_e}}\cdot\underline{n_1}, I_5 = \underline{n_2}\cdot\underline{\underline{B_e}}\cdot\underline{n_2},\ I_6 = \underline{n_3}\cdot\underline{\underline{B_e}}\cdot\underline{n_3} \quad (1)$$

$\underline{n_1}$, $\underline{n_2}$ and $\underline{n_3}$ are the privileged directions for orthotropic properties. Three second order structural tensors $\underline{\underline{A_i}}$ can be calculated with the dyadic product of the preferred directions with themselves:

$$\underline{\underline{A_1}} = \underline{n_1}\otimes\underline{n_1}, \underline{\underline{A_2}} = \underline{n_2}\otimes\underline{n_2}, \underline{\underline{A_3}} = \underline{n_3}\otimes\underline{n_3} \quad (2)$$

In our case, specimen and bottle are shells and we assume that 1 and 2 are the in-plane direction; 3 is the normal direction. Consequently, invariant related to direction 3 are not

Table 2 Increase of the mean temperature during free blowing: for 3 different areas chosen and the mean value

Initial T (°C)	Increase of T (°C) zone 1–2	Increase of T (°C) zone 3–4	Increase of T (°C) zone 5–6	Average of increase of T (°C)
85	16.8	17.2	17.5	17
90	17.1	17.4	17.7	18
95	16.5	17.2	17.6	17
100	16.8	17.5	18.7	18
105	16.2	17.0	17.6	17

used as well as structural tensor $\underline{\underline{A}}_3$. The Hart Smith model chosen to characterize the free energy function writes:

$$\underline{\underline{\sigma}} = -p\underline{\underline{I}} + 2G_1 e^{\Lambda_1(I_1-3)^2}\underline{\underline{B_e}} + 2I_4 G_2 e^{\Lambda_2(I_4-1)^2}\underline{\underline{A_1}} + 2I_5 G_2 e^{\Lambda_2(I_5-1)^2}\underline{\underline{A_2}} \quad (3)$$

Where $\underline{\underline{\sigma}}$ is the Cauchy stress calculated from the strain energy andG_1, G_2, Λ_1 and Λ_2 are parameters of the elastic part of the visco-hyperelastic model. p is the pressure associated to the incompressibility condition of the elastic part.

For the viscous part of the model, we introduce the deviatoric stress tensor $\underline{\underline{\hat{\sigma}}}$:

$$\underline{\underline{\hat{\sigma}}} = 2\eta\underline{\underline{D_v}} \quad \text{that also writes :} \quad \begin{pmatrix} \hat{\sigma}_{11} \\ \hat{\sigma}_{22} \\ \sqrt{2}\sigma_{12} \end{pmatrix} = 2\begin{bmatrix} \eta_{11} & \eta_{12} & 0 \\ \eta_{12} & \eta_{22} & 0 \\ 0 & 0 & \eta_{44} \end{bmatrix}\begin{pmatrix} D_{v11} \\ D_{v22} \\ \sqrt{2}D_{v12} \end{pmatrix} \quad (4)$$

where $\underline{\underline{D_v}}$ is the viscous strain rate. We choose specific h_i functions for each orthotropic direction. In our case, for the bottle description, $i=1$is the hoop direction and $i=2$ the longitudinal one:

$$\begin{cases} \eta_{11} = \eta_0(T)h_1 f\left(\dot{\overline{\varepsilon_v}}\right) \\ \eta_{12} = \beta\eta_0(T)\max(h_1,h_2)f\left(\dot{\overline{\varepsilon_v}}\right) \\ \eta_{22} = \eta_0(T)h_2 f\left(\dot{\overline{\varepsilon_v}}\right) \\ \eta_{44} = \eta_0(T)h\left(\overline{\varepsilon_v}\right)f\left(\dot{\overline{\varepsilon_v}}\right) \end{cases} \quad (5)$$

With:

$$\begin{cases} h_1 = (1-\exp(-K\varepsilon_{v1}))\cdot\exp\left(\alpha_1\left(\frac{\varepsilon_{v1}}{\varepsilon_{vref}(T)}\right)^2 + \alpha_2\left(\frac{\varepsilon_{v1}}{\varepsilon_{vref}(T)}\right) + \alpha_3\right) \\ h_2 = (1-\exp(-K\varepsilon_{v2}))\cdot\exp\left(\alpha_1\left(\frac{\varepsilon_{v2}}{\varepsilon_{vref}(T)}\right)^2 + \alpha_2\left(\frac{\varepsilon_{v1}}{\varepsilon_{vref}(T)}\right) + \alpha_3\right) \end{cases} \quad (6)$$

The expressions of these equations are purely phenomenological one. For Eq. 6 the form is chosen to reproduce the two change of curvature observed on experimental tests. On test, an asymptotic value seems to be reached for elongations but we choose to represent it with an exponential form to avoid numerical problem.

And, coupling with temperature appears through the expressions:

Table 3 The characteristics of the PET

$G(\varepsilon_e)$		G_1	Λ_1	G_2		Λ_2
		2 MPa	1	6 MPa		0.5
$\eta(\varepsilon_v, \dot{\overline{\varepsilon_v}}, T)$	$f\left(\dot{\overline{\varepsilon_v}}\right)$	Λ	A	m		
		10.51	2	0.23		
	$h(\overline{\varepsilon_v})$	η_0	K	α_1	α_2	α_3
		1.4 MPa.s	5.5	5	−2.1	2
	$\eta_0(T)$, $\varepsilon_{vlim}(T)$	C_1	C_2	C_3	C_4	
		1.9	20.31	1.8	180	

$$f\left(\dot{\overline{\varepsilon_v}}\right) = \frac{1}{\left(1+\left(\lambda\dot{\overline{\varepsilon_v}}/\dot{\varepsilon}_{ref}\right)^a\right)^{\frac{1-m}{a}}} \quad (7)$$

$$\ln(\alpha_T) = \frac{-C_1(T-T_{ref})}{C_2+T-T_{ref}}, \quad \eta_0(T) = \alpha_T\eta_0(T_{ref}) \quad (8)$$

$$\varepsilon_{vref}(T) = \frac{\varepsilon_{vref}(T_{ref})}{\exp(-C_3(T-T_{ref})+C_4)} \quad (9)$$

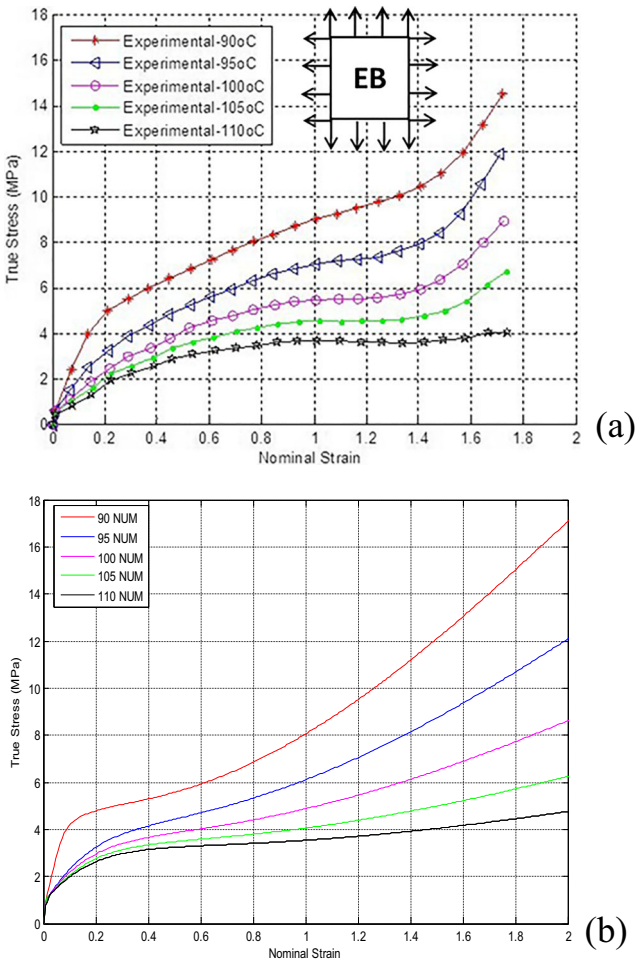

Fig. 5 Comparison between experimental results (**a**) and model simulations (**b**)

where λ, m, a are parameters of the Carreau type function $f\left(\dot{\bar{\varepsilon}}_v\right)$ and $\dot{\varepsilon}_{ref}$ is a reference strain rate that can be taken equal to 1 s^{-1} for sake of simplicity. β is a parameter that indicates the difference between the beginning of the hardening effect in equal biaxial tension test and constant width tension test. From biaxial elongation tests [6] one can identify K, α_1, α_2 and α_3, the parameters of the h function. Variables $\eta_0(T)$ and $\varepsilon_{vref}(T)$ show a significant dependence on temperature. We choose the Williams-Landel-Ferry (WLF) model for the evolution of $\eta_0(T)$. C_1 and C_2 are the WLF parameters, T_{ref}= 90 °C.C_3 and C_4 are parameters in the expression of $\varepsilon_{vref}(T)$.

Therefore, putting together the elastic and viscous expressions of the deviatoric part of the stress tensor, one can obtain:

$$2\eta \underline{\underline{D_v}} = 2G_1 e^{\Lambda_1(I_1-3)^2}\underline{\underline{B_e^{\wedge}}} + 2I_4 G_2 e^{\Lambda_2(I_4-1)^2}\underline{\underline{A_1^{\wedge}}} + 2I_5 G_2 e^{\Lambda_2(I_5-1)^2}\underline{\underline{A_2^{\wedge}}} \quad (10)$$

That leads to:

$$\begin{pmatrix} D_{v11} \\ D_{v22} \\ D_{v12} \end{pmatrix} = \begin{bmatrix} \frac{\eta_{22}}{\eta_{11}\eta_{22}-\eta_{12}^2} & \frac{-\eta_{12}}{\eta_{11}\eta_{22}-\eta_{12}^2} & 0 \\ \frac{-\eta_{12}}{\eta_{11}\eta_{22}-\eta_{12}^2} & \frac{\eta_{22}}{\eta_{11}\eta_{22}-\eta_{12}^2} & 0 \\ 0 & 0 & \frac{1}{\eta_{44}} \end{bmatrix} \begin{pmatrix} \widetilde{d}_{11} \\ \widetilde{d}_{22} \\ \widetilde{d}_{12} \end{pmatrix} \quad (11)$$

Where:

$$\begin{pmatrix} \widetilde{d}_{11} \\ \widetilde{d}_{22} \\ \widetilde{d}_{12} \end{pmatrix} = \left(G_1 e^{\Lambda_1(I_1-3)^2} B_{e11}{}^{\wedge} + G_2 I_4 e^{\Lambda_2(I_4-1)^2} B_{e11}^{\wedge} G_1 e^{\Lambda_1(I_1-3)^2} B_{e22}^{\wedge} + G_2 I_5 e^{\Lambda_2(I_5-1)^2} B_{e22}^{\wedge} G_1 e^{\Lambda_1(I_1-3)^2} B_{e12}^{\wedge} \right) \quad (12)$$

In the following, Eq. 11 is implemented in a finite element code, first to identify the parameters from the tension tests and then, to simulate the ISBM process. Table 3 lists the identified characteristics of the PET near Tg at high strain rate.

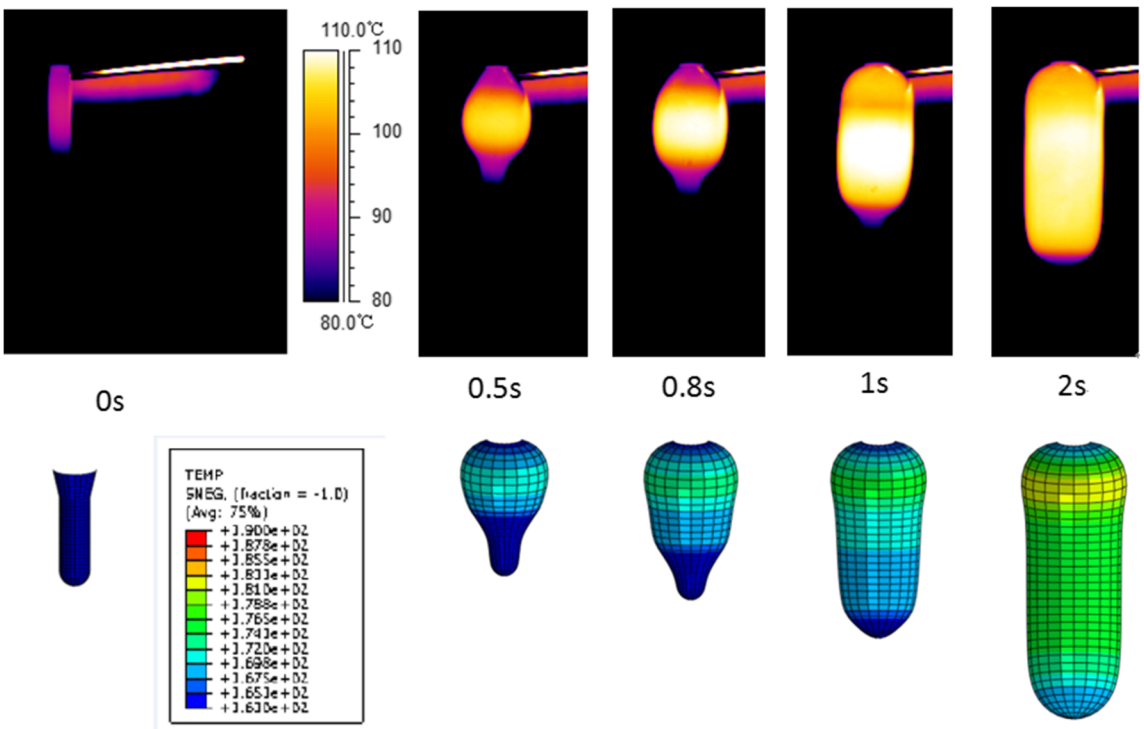

Fig. 6 Comparison between simulation and experimentation for the initial temperature equal to 90 °C. The increase of temperature from thermal camera (upper pictures) and the one from finite element simulation of free blowing (lower snapshots)

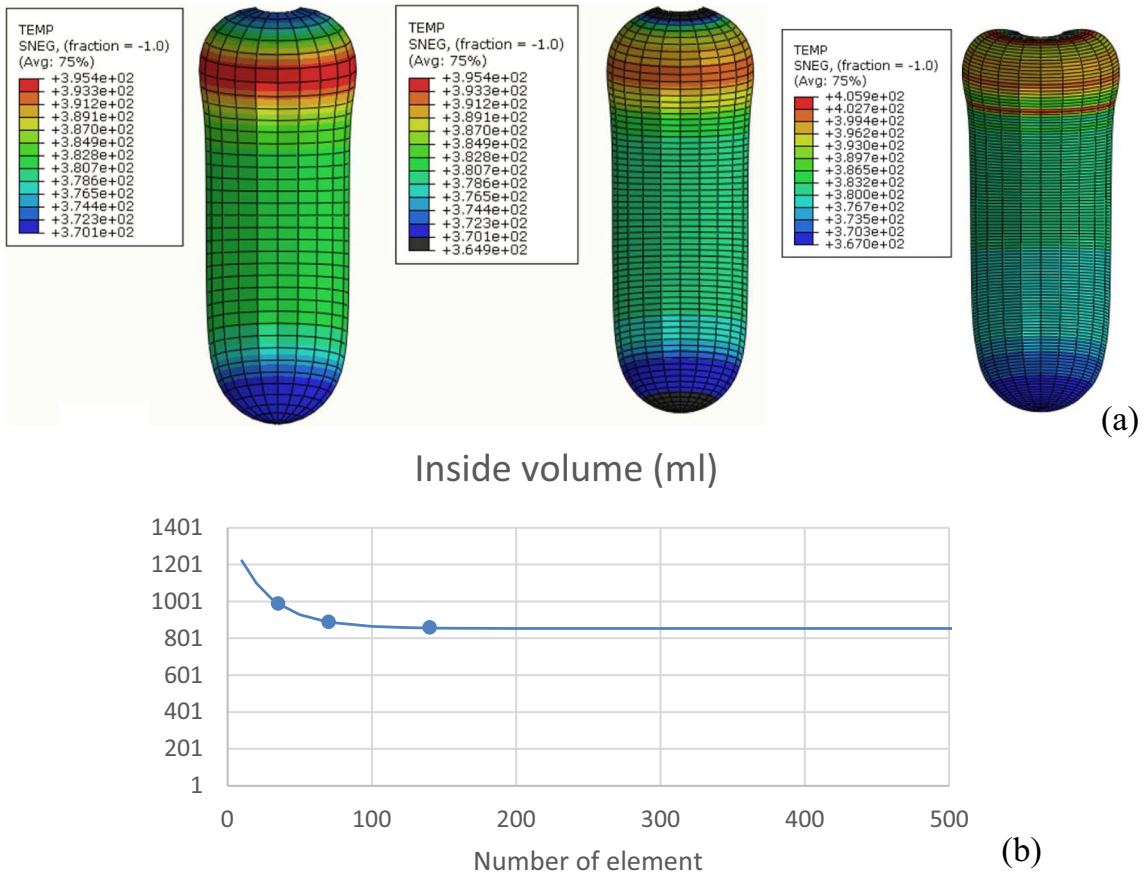

Fig. 7 Influence of mesh refinement on shape evolution (**a**) the final shape is different near the neck and inside volume reduces when number of element increase (**b**) an asymptotic influence of the mesh refinement can be modelled by and exponential function

Identification of the model is managed using experimental data from constant width test and equi-biaxial test. Using the identified parameters one can plot Fig. 5 and compare the numerical and experimental equal biaxial results: strain rate 8 s^{-1} for temperature 90, 95, 100, 105 and 110 °C. For each temperature, the mean difference between numerical results and experimental data does not exceed 20%.

Thermal-mechanical simulation of the free blowing process

The model is implemented into the software ABAQUS / Explicit via a user interface VUMAT [24]. In order to compare the experimental result, we focus on the simulation of the free blowing case. The internal pressure evolution obtained by the manometer from experimental study is implemented as a boundary condition in the simulation. The preform geometry is meshed by 36 shell elements in ABAQUS. The bottle shape and the pressure distribution are axi-symmetric so we use axi-symmetric elements to reduce the number of degrees of freedom of the problem and CPU time. A classical Newton Raphson iterative procedure is used to solve this strongly nonlinear problem.

In order to evaluate the evolution of temperature, we performed a thermal-mechanical simulation. The initial temperature is entered as the initial condition. Because the blowing process is fast (blowing the preform takes less than 5 s) we

Table 4 Increase of temperature (ΔT) under different initial temperature condition

Initial temperature (°C)	Experimental increase of T (°C)	Numerical increase of T (oC)
85	17	17
90	18	17
95	17	19
100	18	18
105	17	18

Table 5 Comparison between the experimental and numerical results

Case		85 °C, 7 bar	90 °C, 6 bar	95 °C, 5.5 bar	100 °C, 4.5 bar	105 °C, 2.5 bar
Elongations						
Experimental	λ_θ top	4.5	4.5	4.8	4.2	4.5
	λ_θ center	4	3.5	3.5	4	4
	λ_θ bottom	4	3.8	3.5	4.3	4
	λ_z top	3.5	4	3.5	4	3.5
	λ_z center	2.5	2.5	2.5	2.5	2.5
	λ_z bottom	3.2	3.5	3.5	3.5	3.7
	Final volume (ml)	920	895	880	900	950
Simulation	λ_θ top	4.5	4.6	4.8	4.6	4.6
	λ_θ center	4	4.6	4.8	4.6	4.6
	λ_θ bottom	3.8	4	4.1	3.9	3.9
	λ_z top	3.8	3.9	3.9	4	4
	λ_z center	3	3	3.8	3.7	3.7
	λ_z bottom	3.4	3.5	3.6	3.4	3.3
	Final volume (ml)	910	990	1060	1010	1000

assume that no heat exchange between the preform and ambient air occurs and that diffusion inside the preform is slow, so that the major contribution to the self heating phenomenon is due to viscous dissipation. The entropy of rubber networks convection or latent heat due to crystallization are neglected so the energy dissipation is evaluated by $\underline{\underline{\sigma}} : \underline{\underline{D_v}}$. Therefore, the thermal part can write as follow:

$$\rho C_p \frac{dT}{dt} = \underline{\underline{\sigma}} : \underline{\underline{D_v}} \tag{13}$$

With $\rho = 1330 kg \cdot m^{-3}$ and $C_p = 1200 J \cdot kg^{-1} \cdot K^{-1}$ for PET material in this range of temperature. Thanks to this thermal-mechanical simulation, one can compare the increase of temperature from numerical simulation with the one obtained during the test for each initial temperature.

As an example, Fig. 6 shows the temperature distribution and the shape evolution from the initial preform to the final bottle. The evolution of temperature during blowing from the finite element simulation is compared to the experimental measurements. In this numerical simulation, the initial temperature is 90 °C and the self heating is about 17 °C in the middle part of the bottle. One can appreciate the similarity of the shape evolution and the temperature distribution.

The influence of the mesh refinement from 35, 70 and 140 elements has been investigated on the case of 90 °C initial temperature. We note an influence on the final volume that shows an asymptotic evolution reported in Fig. 7.

$$V(N) = V_\infty + \left(V_{ref} - V_\infty\right) \exp\left(-\lambda\left(N - N_{ref}\right)\right) \tag{14}$$

Where: $N_{ref} = 35$ elements, $V_{ref} = 990$ ml and $V_\infty = 855$ ml. The evolution fits perfectly with $\lambda = 0.04$. The change of volume is due to the decreasing influence of the mesh on both elongations. The mean increase of temperature is not affected and it remains equal to 16–17 °C. On the other side, the CPU time increases a lot from 5 to 65 h on classical PC. Consequently, we made our discussion on "coarse" mesh.

Table 4 presents the increase of temperature for all tested initial temperature: the increase ΔT does not vary significantly for the chosen cases. For a given initial temperature, one can see that the increase of temperature can reach about 19 °C. One can appreciate the good agreement between the experimental increase measured by the thermal camera with the numerical simulation result.

Table 5 shows the longitudinal and circumferential elongations λ_z and λ_θ in top, center and bottom regions. These are the elongations obtained by numerical simulation; they can be

Table 6 Different "max pressure / initial temperature" cases managed by simulation

T (°C) P (bar)	85	90	95	100	105
7	910 ml	1110 ml	1930 ml	2420 ml	2790 ml
6	700 ml	990 ml	1160 ml	1880 ml	2450 ml
5.5	680 ml	990 ml	1060 ml	1730 ml	2400 ml
4.5	230 ml	760 ml	850 ml	1010 ml	2050 ml
2.5	21 ml	26 ml	460 ml	560 ml	1000 ml

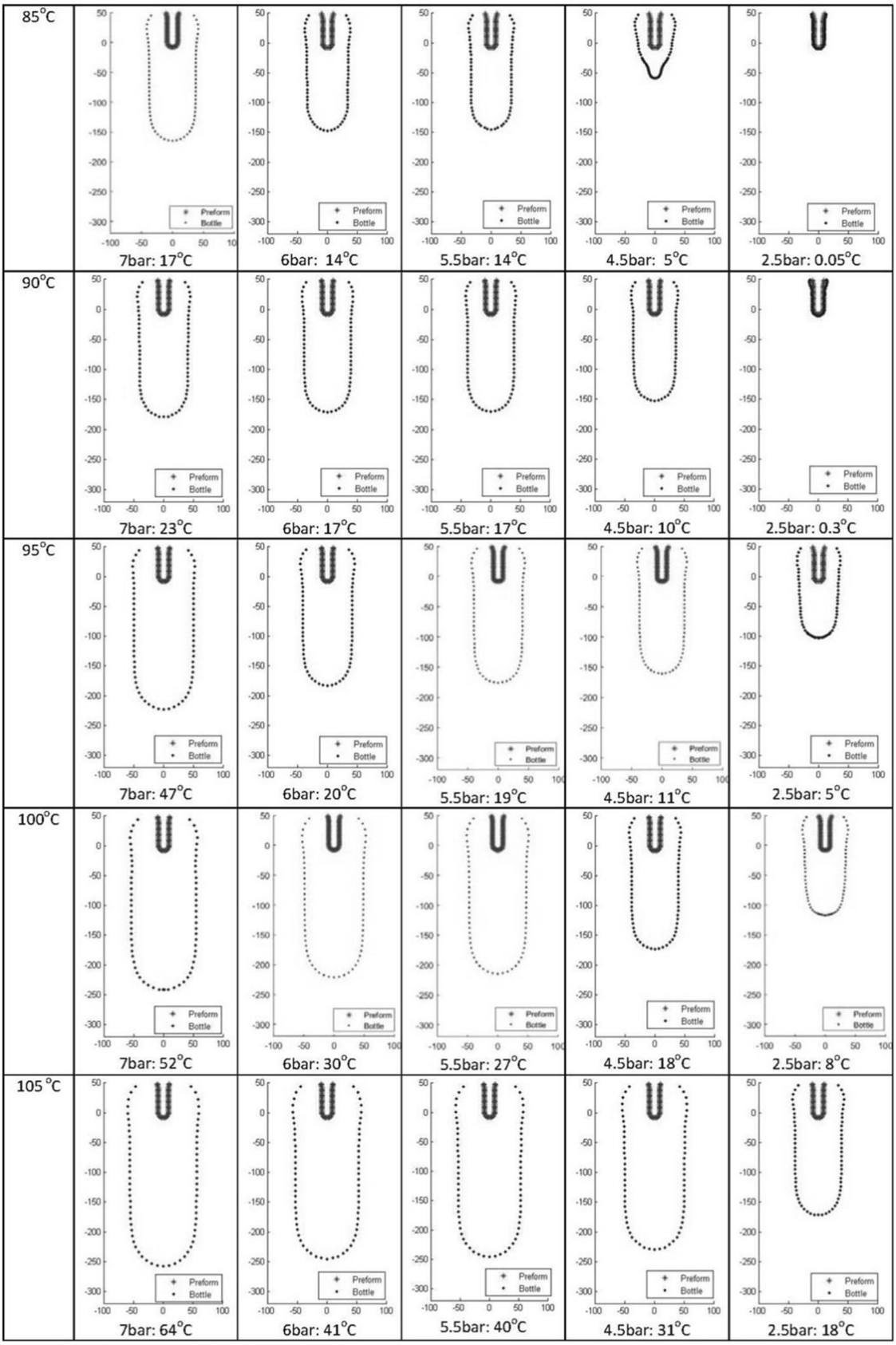

Fig. 8 Final shape and self heating for different pressure and initial temperature

compared to the elongations obtained from experimental measurements.

One can see that the final volume from simulation is a little higher than the experimental one, but the difference is less than 15%: the simulated elongation are higher than the experimental one.

These differences are partially due to the experimental conditions: the initial temperature field, for example, is not uniform on the preform. Natural convection that appears during the tests is not taken into account in the simulation but generates a difference of about 3 °C between the bottom of the preform and the mid region. The difference is also due to the elastic strain recovery: the internal volume is measured when no more pressure is inside while the numerical simulation is managed with pressure until the end.

The pressure decreasing generates an elastic recovery of strain that reduces the inside volume. For example, we consider that this elastic return appears at room temperature for an induced Young modulus of PET around 2000 MPa in longitudinal direction and 3000 MPa in the hoop direction. For 5 bar internal pressure, 50 mm radius ant 0.3 mm thickness, the mean stress can reach 37 MPa in the longitudinal direction and 75 MPa in the hoop direction. Consequently, the longitudinal strain recovery is about 0.17% in longitudinal direction and 0.25% in the hoop one. That leads to a decrease of 7% of the internal ratio and explains half of the difference since no elastic return s taken into account in the simulation.

Numerical simulation helps us to explore different conditions of max pressure and initial temperature in order to confirm the tendency observed experimentally. To that issue, new simulations are managed and results have been summarized in Table 6 and Fig. 8. One can see that, on a wide range, the increase of temperature varies with the pressure. For 85 °C of initial temperature and 2.5 bar pressure, the preform is not stretched and there is no self heating phenomena. For 105 °C of initial temperature and 7 bar pressure, the volume of the blown bottle can reach 2790 ml and the increase of temperature is 64 °C. This case leads to the bottle explosion in the experimental case.

Figure 9 summarizes all results in two graphs that represent the evolution of the mean increase of temperature during the process versus max pressure and the internal volume after blowing versus max pressure. Each curve is corresponding to a different initial temperature. One can see that both series of curves are monotonous even if one can notice a slight plateau around 5-6 bar. This means that there is, in fact an effect of pressure and temperature but the experimental condition chosen were not wide enough to highlight it. One can also notice the correlation between the ΔT evolution and the volume increase and so, when volume is almost equal (as in the experimental series) one can see that the self heating ΔT is also almost constant.

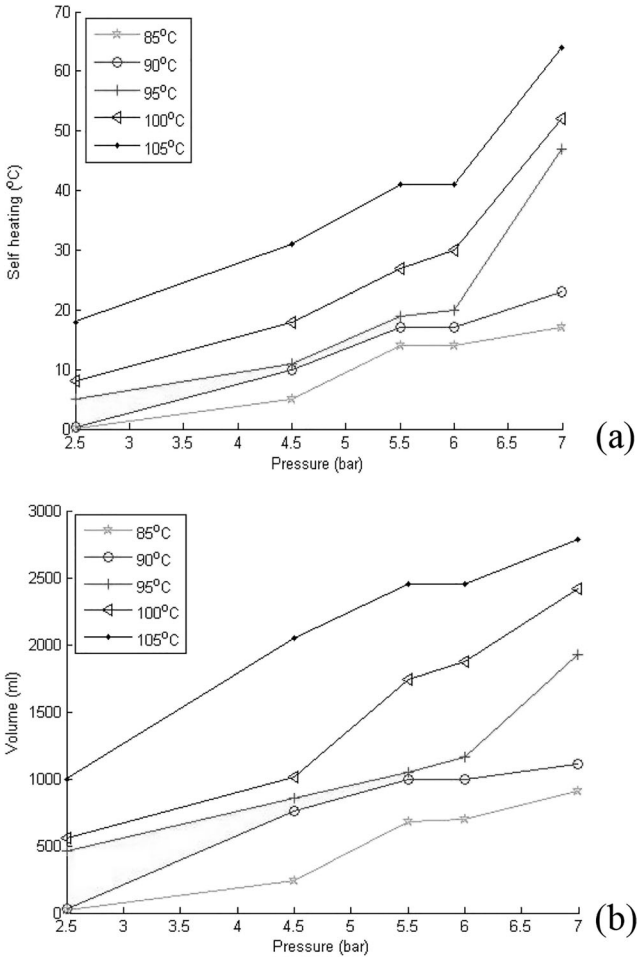

Fig. 9 Effect of pressure on self heating (**a**) and final volume (**b**)

Conclusions

An experimental study on PET preform has been managed: free blowing of preforms at various initial temperature and blowing pressure. In order to compare the self-heating phenomenon, bottles with identical internal volume (with the same final strain applied) were selected and the mean increase of temperature (the self heating) during blowing was measured. We did not detect any influence and that means that only the final strain is involved in the self heating phenomena, independently of the strain rate.

On the other hand, a visco-hyperelastic orthotropic model coupled with the temperature and identified from experimental data of biaxial tension tests, has been computed in a user-interface VUMAT and implemented into the ABAQUS software ABAQUS. We performed free blowing simulations, taking into account the anisotropy and the effect of the temperature. The comparison between self heating measured and self heating obtained from numerical simulation are quasi identical and this validates the toughness of our modelling of the PET behavior near T_g at high strain rates.

As a complement, a complete series of numerical simulation has been achieved using the VHE model and final internal volume and self heating follow the same monotonic evolution versus pressure. That confirms that the self heating phenomena is mainly due to the elongation ratio and not from strain rate. As well, it has been shown that more initial temperature more the volume and the self heating but this has to be nuanced for the range 5-7 bar where self heating does not vary much with pressure.

Compliance with ethical standards

Conflict of interest The authors declare that they have no conflict of interest.

References

1. Yousefi A, DiRaddo R, Bendada A Simulation of the mobile preform reheat in injection stretch blow moulding process. Polymer Proceeding Society 17. Montreal, Canada. May 21–24 2001
2. Haung HX, Yin ZS, Liu JH (2007) Visualisation study and analysis on preform growth in polyethylene terephthalate stretch blow moulding. J Appl Polym Sci 103(1):564–573
3. Billon N, Erner A, Gorlier E (2005) Kinematics of stretch blow moulding and plug assisted thermoforming of polymers; experimental study, Polymer Proceeding Society 21. Leipzig, Germany
4. Nagarjappa CC (2012) PhD. Thesis, Developing and validating stretch blow moulding simulation through free blow experiments, Queens University Belfast, School of Mechanical & Aerospace Engineering
5. Menary GH, Tan CW, Harkin-Jones EMA, Armstrong CG, Martin PJ (2012) Biaxial deformation of PET at conditions applicable to the stretch blow molding process. Polym Eng Sci 52(3):671–688
6. Chevalier L, Luo YM, Monteiro E, Menary G (2012) Onvisco-elastic modelling of polyethylene terephthalate behaviour during multiaxial elongations slightly over the glass transition temperature. Mech Mater 52:103–116
7. Luo YM, Chevalier L (2019) On induced properties and self heating during free blowing of PET preform. Int Polym Process 34(3):330–338
8. Marco Y (2003) Caractérisation Multi-Axiale du Comportement et de la Micro-Structure d'un Semi-Cristallin: Application au Cas du P.E.T., PhD Thesis, ENS Cachan, Cachan
9. Bedoui F (2005) Etude du Comportement Elastique et Viscoélastique Linéaire des Polymères Semi-Cristallins par Approche Micromécanique, PhD Thesis, ENSAM, Paris
10. Gong YH (2018) Sur l'Analyse Multiéchelle du Changement de Morphologie du PET sous l'effet de la Température ou des Sollicitations Mécaniques, PhD Thesis, University Paris-Est, Marne-la-Vallée
11. Lebaudy P, Saiter JM, Grenet J, Vautier C (1995) Temperature distribution in poly(ethylene terephthalate) plate undergoing heat treatment. Diffusion Influence and Application, Polymer 36(6): 1217–1221
12. Schmidt FM, Le Maoult Y, Monteix S (2003) Modelling of infrared heating of thermoplastic sheet used in thermoforming process. J Mater Process Technol 143–144:225–231
13. Monteix S, Schmidt F, Le Maoult Y (2001) Experimental study and numerical simulation of preform or sheet exposed to infrared radiative heating. J Mater Process Technol 119(1–3):90–97
14. Huang HX, Li YZ, Deng YH (2006) Online real-time acquisition for transient temperature in blow molding. Polym Test 25(6):839–845
15. Salomeia YM, Menary GH, Armstrong CG (2013) Experimental investigation of stretch blow molding, part 1: instrumentation in an industrial environment. Advances in Polymer Technology 32(S1): E771–E783
16. Menary G (2012) The effect of temperature, strain rate and strain on the induced mechanical properties of Biaxially stretched PET. The 17th annual ESAFORM conference on material forming, Erlangen, German, 14–16 March 2012
17. Huang H-X, Deng Y-H, Huang Y-F (2005) Temperature profiles within reheated preform in stretch blow molding. ANTEC'05, Boston, Massachusetts
18. Champin C (2007) Modélisation 3D du chauffage par rayonnement infrarouge et de l'étirage soufflage de corps creux en P.E.T., PhD thesis, Ecole Nationale Supérieure des Mines de Paris
19. Michaeli W, Papst W (2004) FE-Analysis of the Two-Step Stretch Blow Molding Process. in SPE ANTEC Technical Papers 30 , Chicago, USA
20. Martin L, Stracovsky D, Laroche D, Bardetti A, Ben-Yedder R, DiRaddo R (1999) Modeling and experimental validation of the stretch blow molding of PET. In SPE ANTEC Technical Papers, New York
21. Cosson B, Schmidt F, Le Maoult Y, Bordival M (2011) Infrared heating stage simulation of semi-transparent media (PET) using ray tracing method. Int J Mater Form 4(1):1–10
22. Luo YM, Chevalier L, Utheza F, Monteiro E (2013) Numerical simulation of the thermodependant visco-hyperelastic behaviour of PET near the Glass Transition Temperature: prediction of the self heating during biaxail tension test, Polymer Eng. & Science, on line
23. Luo YM, Chevalier L, Utheza F, Nicolas X (2014) Simplified modelling of the infrared heating involving the air convection effect before the injection stretch blowing moulding of PET preform, ESAFORM, Espoo, Finland, May 2014
24. Luo YM, Chevalier L, Monteiro E, Utheza F (2017) Self heating during stretch blow molding: an experimental numerical comparison, the 20th international ESAFORM conference on material forming, Dublin, Ireland, April 26-28, 2017
25. Schmidt FM, Agassant JF, Bellet M (1998) Experimental study and numerical simulation of the injection stretch/blow moulding process. Poly Eng Sci 38(9):1399–1412
26. Menary GH, Tan CW, Picard M, Billon N Armstrong CG, Harkin-Jones EMA (2007) Numerical simulation of injection stretch blow moulding: comparison with experimental free blow trials. 10th ESAFORM conference on material forming, AIPConf Proc, vol 907, pp 939–944
27. Salomeia YM (2009) PhD Thesis, Improved understanding of injection stretch blow moulding through instrumentation, process monitoring and modelling. Queen's University of Belfast, School of mechanical & Aerospace Engineering
28. Bordival M, Schmidt FM, Le Maoult Y, Velay V (2009) Optimization of preform temperature distribution for stretch-blow moulding of PET bottles: infrared heating and blowing modelling. Polym Eng Sci 49(4):783–793
29. Nixon J, Menary GH, Yan S (2017) Finite element simulations of stretch-blow moulding with experimental validation over a broad process window. Int J Mater Form 10(5):793–809
30. Barakos G, Mitsoulis E (1996) Non-isothermal viscoelastic simulations of extrusion through dies and prediction of the bending phenomenon. J Nonnewton Fluid Mech 62(1):55–79
31. Marckman G, Verron E, Peseux B (2001) Finite element analysis of blow molding and thermoforming using a dynamic explicit procedure. Polym Eng Sci 41(3):426–439

32. Buckley CP, Jones DP (1996) Hot-drawing of poly(ethylene terephthalate) under biaxial stress: application of a three-dimensional glass-rubber constitutive model. Polymer 37(12):2403–2414
33. Luo Y-M, Chevalier L, Monteiro E, Yan S, Menary G (2020) Simulation of the injection stretch blow moulding process: an anisotropic visco-hyperelastic model for PET behavior. Polym Eng Sci 60(4):823–831